Electrochimica Acta 100 (2013) 85–92

Contents lists available at SciVerse ScienceDirect

Electrochimica Acta

journal homepage: www.elsevier.com/locate/electacta

Promotion of charge transport in low-temperature fabricated TiO_2 electrodes by curing-induced compression stress

Jiazang Chen, Jianqiang Luo, Xihai Jin, Yangqiao Liu, Jing Sun*, Lian Gao

State Key Laboratory of High Performance Ceramics and Superfine Microstructure, Shanghai Institute of Ceramics, Chinese Academy of Sciences, Shanghai 200050, China

ARTICLE INFO

Article history:
Received 12 November 2012
Received in revised form 4 March 2013
Accepted 23 March 2013
Available online 30 March 2013

Keywords:
Charge transport
Charge recombination
Strain
Curing
Dye-sensitized solar cells

ABSTRACT

In low-temperature fabricated dye-sensitized solar cells, promotion of the interparticle electronic connectivity, reduction of the trapping/detrapping events, and suppression of charge recombination on the semiconductor–electrolyte interface are key steps to improve charge collection and energy conversion efficiency. In this work, a new method based on curing cementing material ($Ca(OH)_2$) under CO_2 ambient to produce uniform $CaCO_3$ coatings on mesoporous TiO_2 nanoparticulate films is presented. The volume shrinkage resulting from the phase conversion of calcareous coating during the curing procedure can produce strong strain on the TiO_2 electrode. By virtue of the compression stress, the interparticle electronic connectivity was promoted and the density of electronic states in the bandgap of the semiconductor was reduced. Thus, the electrode with $CaCO_3$ coating exhibits better performance for diffusion and collection of electrons. Moreover, the formed $CaCO_3$ coatings can also prevent the electrons from recombination on the semiconductor–electrolyte interface. In combination with a platinized electrode and electrolyte, the photovoltaic devices with $CaCO_3$ coated electrode achieved an energy conversion efficiency of 4.79%, which is 40% higher than that of the cell with blank electrode.

1. Introduction

Dye-sensitized solar cells (DSSCs) have been considered as promising alternatives to the conventional crystalline-silicon solar cells on account of their low-cost, facile fabrication and relatively high energy conversion efficiency [1–4]. In particular, fabrication of DSSCs on plastic substrate has the potentials to extend their application and to compatible with the roll-to-roll production process. However, one of the obstacles for the flexible DSSCs (*f*-DSSCs) is that the instability of plastic substrate above 200 °C prevents any high-temperature (400–550 °C) sintering process, which is critically important to form high connectivity between TiO_2 particles. And certain problems, such as poor charge transfer between individual particles, high density of electronic trap in the bandgap of the low-temperature (usually lower than 150 °C) sintered semiconductor films will lower the diffusion coefficient and diffusion length of electrons, which directly restrict the photovoltaic performance. Thus, it is of great importance to develop low-temperature fabrication techniques for efficient semiconductor electrodes.

In order to improve the photoelectrochemical performance of the semiconductor electrodes, many preparation and post-treatment techniques, such as chemical sintering [5–9], electrospray [10], electrodeposition [11,12], treatment of pastes or electrodes with titanium-containing gel/solution [13,14], mechanical compression of the semiconductor films [15,16], and formation of surface coating on the electrodes have been developed [17–19]. These techniques are mainly striving to increase the interparticle necking area to promote the charge transfer between the nanoparticles [13,14,16], while large amount of the electronic states in the bandgap is still remained in the semiconductor. The residual sites of electronic states in the electrode will act as electron traps during the charge transport, resulting in a lower electron diffusion coefficient and poorer charge collection efficiency. Surface coating is able to passivate the surface states and reduce the interfacial charge recombination [13,14,16]. However, further improvement in charge transport in the electrode is still needed.

In this work, we propose a new method to improve the charge transport performance of the low-temperature sintered TiO_2 films by introduction of a special coating on the electrode surface. The coating was formed by successive ion layers adsorption and reaction (SILAR) of $Ca(OH)_2$ on the surface of the TiO_2 electrodes followed by curing under CO_2 ambient (Fig. 1). We found that the strain resulting from the phase conversion of the calcareous coating is able to promote the interparticle electronic connectivity and reduce the density of electronic states in the bandgap of the semiconductor electrodes, which will facilitate the charge transport and collection.

* Corresponding author. Tel.: +86 21 52412722; fax: +86 21 52413122.
E-mail address: jingsun@mail.sic.ac.cn (J. Sun).

0013-4686/$ – see front matter © 2013 Elsevier Ltd. All rights reserved.
http://dx.doi.org/10.1016/j.electacta.2013.03.127

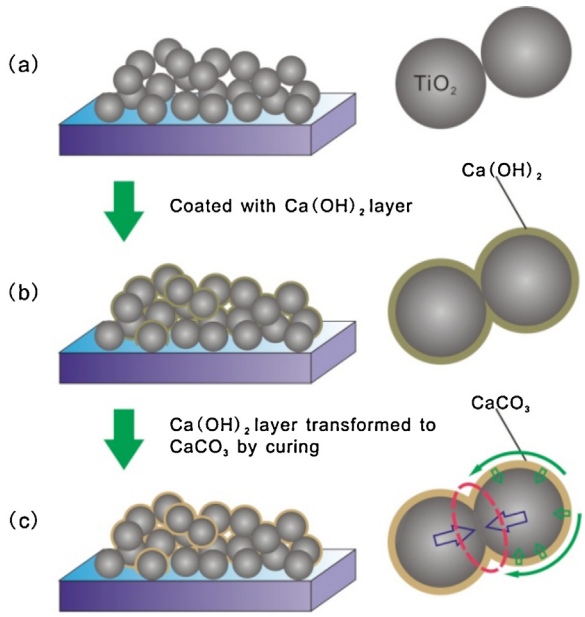

Fig. 1. Schematic diagram for coating and curing $Ca(OH)_2$ layers on the surface of the low-temperature formed porous TiO_2 electrodes. The right side of the figure shows the change of the interaction condition between the TiO_2 nanoparticles. The right side in (c) shows the promotion of TiO_2 interparticle connectivity by the volume shrinkage strain result from the phase conversion of calcareous layers.

2. Development of curing for low temperature fabrication of TiO_2 electrode

For efficient *f*-DSSCs, promotion of electronic connectivity between individual particles, creation of barrier layers on the semiconductor electrode surface, and reduction of density of intraband electronic states are essential approaches to facilitate interparticle charge transfer, suppress interfacial charge recombination, and lower the probability of trapping/detrapping events during electron transport, respectively. Besides, in order to avoid the contamination of the electrodes, all the auxiliary materials should be easily removed, and introduction or production of insoluble organic species should be minimized during the electrode fabrication [18].

$Ca(OH)_2$ is a common cementing material, which is widely used as binder in construction industry. $Ca(OH)_2$ can be cured in the presence of CO_2 and transformed into $CaCO_3$, producing a strong volume shrinkage [20–23]. $CaCO_3$ coated TiO_2 electrode can be obtained by SILAR of $Ca(OH)_2$ on the surface of TiO_2 electrodes followed by curing under CO_2 ambient. The potential volume shrinkage of the calcareous layers would force the formed $CaCO_3$ coatings to tightly coat on the surface of the electrode (Fig. 1). Thus, the $CaCO_3$ coating could bring strong strain on the electrode. The strain resulting from the volume shrinkage occurred during the phase conversion of calcareous layers would simultaneously promote the interparticle necking condition and bring a compression stress to the TiO_2 building blocks themselves.

Besides, it has been revealed that the $CaCO_3$ coatings on the TiO_2 electrodes surface can protect the electrons from recombination, since the energy level of conduction band edge of the calcareous layers is much higher than that of TiO_2 semiconductor [24,25]. And the formed $CaCO_3$ coating can passivate the surface states on the TiO_2 electrode, which can reduce the electrons from recombination intermediated *via* the trap sites (Fig. 2).

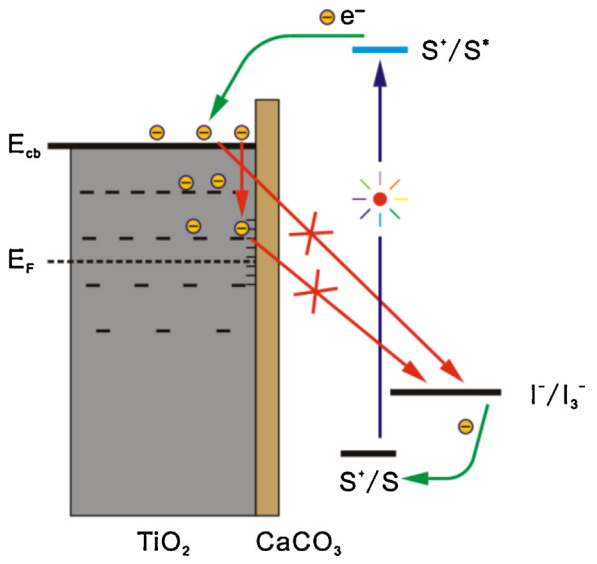

Fig. 2. Scheme for the energy level diagram of DSSC with calcareous layers on the mesoporous TiO_2 electrode. The $CaCO_3$ coatings can effectively prevent the charge recombination between the electrons in the semiconductor electrode and electron acceptors (i.e. I_3^- ions).

3. Experimental

3.1. Fabrication of TiO_2 electrodes

Fabrication of mesoporous TiO_2 electrodes was mainly according to a literature procedure [26]. The paste consisting of 3 g of TiO_2 (Degussa P25) powders, 5 mL of ethanol, and 5 mL of water was ball milled for 12 h. The TiO_2 paste was then deposited by doctor blade technique on fluorine-doped tin dioxide (FTO) glass by preparing an active area of 0.38 cm^2. The TiO_2 film was then sintered at 150 °C for 12 h. SILAR of $Ca(OH)_2$ onto the surface of the TiO_2 electrode was performed by immersing the semiconductor electrodes into a 0.1 M $Ca(NO_3)_2$ in ethanol for 3 h. After absorption of the calcareous ions, the electrode was then immersed into a 0.2 M NaOH in ethanol for 3 h.

After SILAR of $Ca(OH)_2$, the electrodes were moved to a sealed curing box (Fig. 3) to cure. The required CO_2 and moisture for curing the $Ca(OH)_2$ were supplied by bubbling the water using the CO_2 stream in a sealed bottle, which is connected with the curing box. The temperature for the curing ambient was modulated by the hot plate. Curing of the $Ca(OH)_2$ into $CaCO_3$ was performed at the temperature of 80 °C for 30 h. After curing, the electrodes were rinsed with water to remove the unreacted $Ca(OH)_2$.

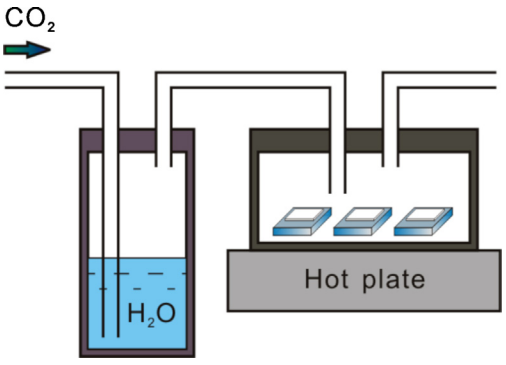

Fig. 3. Schematic diagram for the curing equip and the experimental conditions. The required moisture was supplied by bubbling the water using the CO_2 curing gas. The temperature for the curing condition can be adjusted by the hot plate.

Transmission electron microscopy (TEM) was employed to determine the formation of the calcareous coating by performing a JEM-2100 electron microscope operated at 200 kV. The morphologies of the electrodes were characterized by scanning electron microscopy (SEM) carried out on an S-4800 electron microscope. X-ray photoelectron spectroscopy (XPS) was employed to characterize the bonding properties of the TiO_2 films using an ESCALAB 250 spectrometer.

3.2. Assembly of DSSCs

Sensitization of the semiconductor films was firstly carried out by heating these TiO_2-based electrodes at 120 °C, after cooling to 80 °C, the TiO_2 electrode was immersed overnight in a ruthenium dye solution (cis-di(thiocyanato)-N,N′-bis(2,2′-bipyridyl-4-carboxyl acid-4′-tetrabutylammonium carboxylate) ruthenium (II) (also known as N-719) that was dissolved in acetonitrile with a concentration of 0.5 mM). The electrode was then rinsed with acetonitrile and dried. Then one drop of iodine-containing electrolyte was deposited onto the surface of the electrode and penetrated inside the TiO_2 film *via* capillary action. The electrolyte was composed of 0.1 M lithium iodide (LiI), 0.6 M tetrabutylammonium iodide (TBAI), 0.05 M iodine (I_2), and 0.5 M 4-tert-butylpyridine dissolved in acetonitrile. A platinized FTO counter electrode was then clipped onto the top of TiO_2 photoelectrode to form photovoltaic device.

3.3. Electrochemistry and photoelectrochemistry

The photovoltaic properties of the DSSCs were characterized by recording the photocurrent–voltage (*I–V*) curves under illumination of A.M. 1.5 G (100 mW/cm^2). The illumination was provided by performing an Oriel-Newport solar simulator. Electrochemical impedance spectroscopy (EIS) measurements were carried out by performing a computer-controlled potentiostat (PAR 2273). The obtained spectra were fitted with Z-view software. To determine the flat band potential of the electrode, potentiodyanmic impedance spectroscopy was performed in a tri-electrode system using semiconductor films as the working electrode, a platinum sheet and a saturated calomel electrode (SCE) were employed as the counter electrode and reference electrode, respectively. Electrolyte containing 0.1 M NaOH and 0.1 M Na_2SO_4 aqueous solution was used and nitrogen bubbling was carried out before taking the measurement. Transient spectroscopic measurements were carried out by using a light-emitting diode (white light) or laser diode (CNI-CIOMP, λ = 635 nm) providing light that was incident on the FTO front contact of the cells. Electron lifetime, τ_n of the cells was determined by monitoring the variation of open-circuit voltage with time in terms of the expression [27]:

$$\tau_n = -\frac{k_B T}{e}\left(\frac{dV_{OC}}{dt}\right)^{-1} \quad (1)$$

Estimation of the effective electron diffusion coefficient was performed by photocurrent transient measurement according to a literature procedure [28]. The data were obtained by stepped light-induced transient measurement of photocurrents. The time constant was obtained by fitting the decay of the photocurrent transient to the function of $\exp(-t/\tau_c)$, where t is time and τ_c is the time constant for electron collection. The values of D_n can be obtained by the expression: $D_n = L^2/(2.35 * \tau_c)$, where L is the thickness of the semiconductor films. In order to estimate the charge accumulated in the semiconductor electrodes, a charge extraction method based on potential step chronoamperometry was employed [29,30]. Measurement of the density of trapped electrons in the semiconductor electrode was carried out on a CH Instrument (CHI660D).

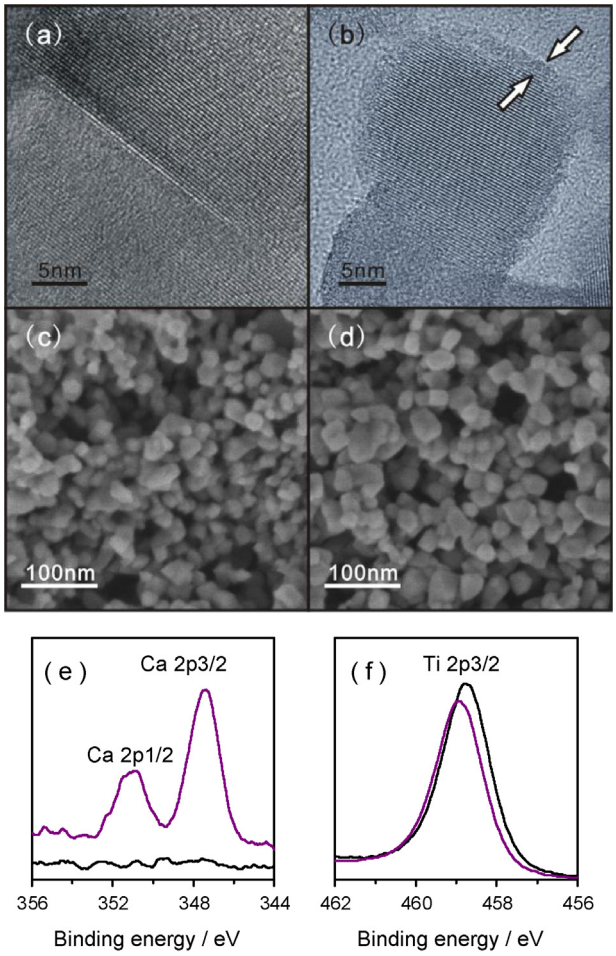

Fig. 4. Characterizations of the TiO_2 electrodes. TEM images showing the surface of the blank TiO_2 nanoparticles (a) and the nanoparticles homogeneously coated with cured calcareous coatings (marked by the white arrows in (b)). SEM images for the blank (c) and cured (d) TiO_2 porous electrodes. The shape of the building blocks becomes "fat" after the calcareous layers were coated and cured (c and d). High-resolution XPS patterns of Ca 2p (e) and Ti $2p_{3/2}$ (f) for the blank (black line) and cured $CaCO_3$ coated (purple line) TiO_2 films.

4. Results and discussion

4.1. General characterizations of materials

The morphologies and structures of the TiO_2 electrodes and materials were characterized by SEM and TEM. Fig. 4(a) is the TEM image taken on the edge of the TiO_2 (P25) particles without coating, in which the surface facets of the nanocrystal are clearly shown. After SILAR of $Ca(OH)_2$ and curing under CO_2 ambient, the TiO_2 (P25) particles were tightly coated by a very uniform, compact and continuous conformal calcareous shell (Fig. 4(b)). The morphologies of the building blocks in the electrodes before and after modification of $CaCO_3$ are also investigated by SEM characterizations (Fig. 4(c and d)). It can be seen that TiO_2 nanostructures remain their intrinsic morphologies in the cured electrodes, indicating the deposited $Ca(OH)_2$ layers and the following cured $CaCO_3$ coating was uniformly templated by the TiO_2 skeletons. Fig. 4(e and f) shows the high-resolution XPS pattern of the TiO_2 films. The Ca $2p_{1/2}$ and Ca $2p_{3/2}$ peaks respectively detected at approximately 351 and 347.5 eV can be assigned to the binding energy of calcium in the $CaCO_3$. The Ti $2p_{3/2}$ spectra for the two samples were also recorded (Fig. 4(f)). The position of the Ti $2p_{3/2}$ peak for the $CaCO_3$ coated sample exhibits a slight shift toward a higher

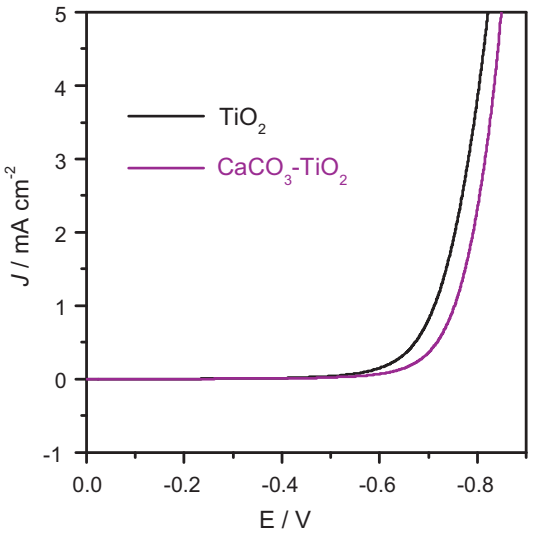

Fig. 5. Effect of cured calcareous coatings on the voltammetric behaviors of the cells.

binding energy. The interactions between the calcareous coating and the Ti ions and the redistribution of electronic cloud between surface elements may contribute to the change of chemical environment and the chemical shift.

4.2. Band edge movement and surface passivation

4.2.1. General voltammetric characteristics of calcareous coatings

In order to preliminarily determine the validity of cured $CaCO_3$ coatings, voltammetry and impedance spectroscopy were adopted to investigate the electrochemical behaviors of the semiconductor electrode. In the dark condition, the voltammetry behaviors are strongly dependent on the distribution and density of localized states, and in particular, the position of conduction band edge of the semiconductor electrodes. Under forward bias, cathodic current arises from reduction of the I_3^- ions in the electrolyte by electrons injected from the TCO substrate into the mesoporous semiconductor. The result current, represents the recombination of the charge carriers on the semiconductor-electrolyte interface (SEI), is consisting of the direct transfer of the conduction band electrons to the electron acceptors in the electrolyte, and the electronic process intermediated by the trap sites on the surface of the semiconductor [31,32].

Fig. 5 shows the voltammetry curves of the cells with blank and cured electrodes. As it shows, the onset potential for the cured cell is more negative than that of the blank one, suggesting the conduction band (edge) position of the cured semiconductor electrode is higher, as compared with that of the blank one. By careful inspection of the voltammetry behaviors, it can be seen that the two curves exhibit different slopes when the biases are beyond the respective onset potentials. For the cell with cured electrode, the slope for the variation of current over the potential range is slightly larger, as compared with that of blank one, suggesting that the current mediated by traps becomes less dominant. Thus, the introduction of the calcareous coatings on the surface can suppress the charge recombination *via* the surface states, and improve the quality of the semiconductor–electrolyte junction. Further evidences for the band edge movement and surface passivation were obtained by comparing the flat band potentials and transfer constant for the interfacial charge recombination of the electrodes.

4.2.2. Surface passivation and interfacial charge transfer retardation

In order to take a further insight into the surface of semiconductor electrode, the feature of the interfacial charge recombination was investigated. The charge recombination on the SEI can be described by the value of charge transfer resistance (R_{ct}), which can be obtained from impedance results. Fig. 6(a) presents the typical impedance pattern of DSSCs. The R_{ct} value can be obtained by fitting the EIS patterns using the transmission line model (inset of Fig. 6(a)) developed by Bisquert et al. [33–36].

Fig. 6(b) presents SEI charge transfer resistance, R_{ct} of the cells with blank and cured TiO_2 electrodes. It can be see that the R_{ct} values decreased exponentially as the Fermi level move toward the conduction band, indicating that charge transfer rate increased as the density of electron increase. By comparing the two curves, it is clear that the charge transfer resistance significantly increased after modification of the cured calcareous coatings.

In order to further confirm the quality of the semiconductor, transfer constant for the charge recombination of the SEI was evaluated. Transfer constant for interfacial charge recombination corresponds to the reciprocal value of the diode quality factor. Here we obtain the transfer constant with the following expression

$$R_{ct} = R_{ct,0} \exp\left[-\frac{e\beta}{k_B T} V\right] \quad (2)$$

where β is the transfer constant. The direct transfer of electron from the conduction band edge to the hole carriers in the electrolyte should give $\beta = 1$. The transfer constants evaluated from Eq. (2) are 0.44 and 0.50 for the blank and cured electrodes, respectively, corresponding to the diode quality factor of 2.26 and 1.97. The high quality of the cured electrode suggests that the surface states were effectively passivated and the transfer of electron intermediated by these sites become less predominant.

4.2.3. Band edge movement

Fig. 7 presents Mott–Schottky (MS) plots for the cell with blank and cured TiO_2 electrodes obtained by performing potentiodynamic electrochemical impedance spectroscopy. The effective doping concentration in the space charge layer and the flat band potential of semiconductor can be calculated in terms of the expression:

$$\frac{1}{C^2} = \frac{2}{\varepsilon\varepsilon_0 e_0 N_D}\left(\varphi - \varphi_{fb} - \frac{k_B T}{e_0}\right) \quad (3)$$

where φ_{fb} is the so-called flat band potential, that is the applied potential (φ) at which the semiconductor energy band are "flat", N_D, the doping density, k_B, the Boltzmman constant, T, the temperature, ε, the relative dielectric constant of the semiconductor, ε_0, permittivity of free space. The slope is inversely proportional to the effective donor concentration in the space charge layer of semiconductor, and the flat band potential can be determined by extrapolation to $C^{-2} = 0$. The calculated flat band potentials are −0.653 V for the blank electrode and −0.687 V for the cured one. The donor concentration of the blank and cured electrodes was calculated to be 2.88×10^{18} and 2.02×10^{18} cm^{-3}, respectively, using a linear fitting method.

It has been reported that the basicity (or acidity) of the coatings has strong influence to the flat band potential of host semiconductor [37,38]. For example, by modification of basic materials onto the semiconductor electrodes, the formed interfacial dipoles will deprotonate the surface of the host semiconductor, result in a negative shift of flat band potential [37]. In our system, the isoelectric point of $CaCO_3$ (pH 8.3) is higher than that of TiO_2 (pH 6.2) [39]. The negative shift of 34 mV in the flat potentials for the cured TiO_2 electrodes suggests that the calcareous coatings are tightly contacting with the host semiconductor. The depleted (dielectric) state

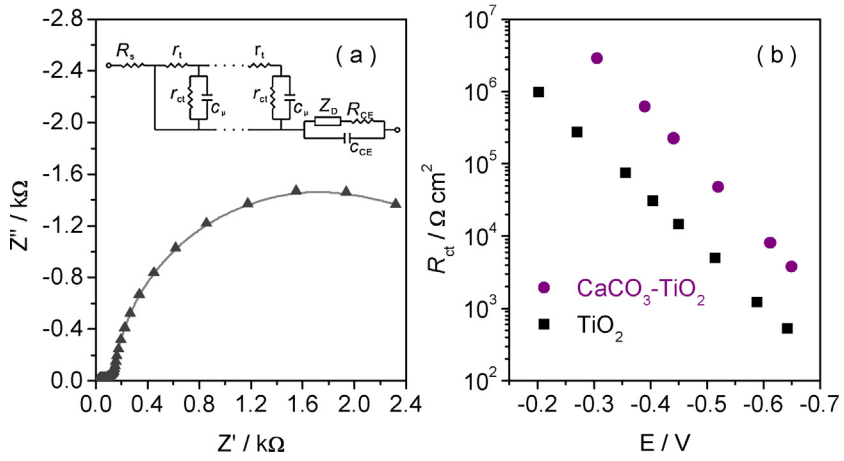

Fig. 6. (a) Typical impedance spectrum for dye-sensitized solar cells. (b) Effect of $CaCO_3$ coatings on the interfacial charge recombination between electrons and triiodide ions. The values of R_{ct} were estimated from impedance patterns.

remains at more negative potential for the cured TiO_2 electrodes reflects that band edge movement toward higher energy level occurred. Moreover, it is noteworthy that the calculated donor density, which is proportional to the differential capacitance according to Eq. (3), is slightly lowered after curing. The differential capacitance, C measured by potentiodynamic impedance spectroscopy is, in fact, the sum of the capacitance contributed by the space charge (C_{SC}) and the electronic states in the surface of the semiconductor (C_{SS}) connected in parallel (C_{SC} || C_{SS}) [40]. The decrease in differential capacitance suggests that the contribution from the surface states is smaller, resulting most likely from the passivation of the surface states of the TiO_2 electrode by the $CaCO_3$ coatings.

4.3. Strain promoted charge transport

4.3.1. Improvement in the diffusion of electrons in the semiconductor electrodes

The electronic processes, including the transport of charge in the porous TiO_2 electrode occurs *via* diffusion driven by electron concentration gradient and the recombination of electrons with the oxidized species on SEI, are strongly influenced by the density and distribution of electronic states in the bandgap of the semiconductor. Under illumination, transport of electrons in the semiconductor of DSSCs strongly depends on light intensity because of the broad distribution of bandgap traps [41,42]. In the model of multiple trapping (MT) framework, transport of electrons through extended states is slowed down by trapping/detrapping events, while direct hopping between localized states is neglected [43–50]. The waiting time for the thermal release of electrons to the extended state strongly influences the time constant of charge transport. Therefore, the effective diffusion coefficient, D_n of electrons is decided by the density of localized state and the depth of the trap sites:

$$D_n = \left(\frac{\partial n_c}{\partial n_t}\right) D_0 \tag{4}$$

where D_0 is the diffusion coefficient of electrons at energy level of conduction band edge.

Fig. 8 presents the evaluated electron collection-time constant and diffusion parameter for each electrode plotted *versus* photocurrent. It is clear that the introduction of calcareous coatings significantly influences the charge transport parameters. In all the measured range, the cured electrode exhibits significantly large diffusion coefficient for electrons transport in the semiconductor, as compared with the blank electrode. For example, in the high current range, the values of D_n for the cured electrode are about two times larger than that of the blank one. As the densities of the photocurrent become lower, the charge diffusion parameters for both of the two electrodes decreased. By comparing the two plots (Fig. 8(b)), it can be seen that the slope of D_n–J_{SC} relationship for the electrode with calcareous coatings is relatively low, which suggests that the decrease in the charge diffusion coefficient over the current density is not obvious, as compared with that of the blank one.

In the high photocurrent range, most of the trap sites were occupied by the electrons, since the density of the photogenerated charge carrier in the semiconductor electrode is high. In this situation, the influence of trapping/detrapping event on the charge diffusion coefficient is not obvious (for both the blank and cured electrodes). Thus, the larger diffusion coefficient for the cured electrode should be attributed to the improvement in the charge transfer performance between individual particles, resulting most likely from the promoted interparticle electronic connectivity by the phase conversion generated compression stress of the calcareous coatings. The improvement in the contact condition between the adjacent particles is in excellent agreement with our expected assumption (Fig. 1).

As the photocurrent density decreasing, namely the density of photogenerated electrons in the semiconductor becoming lower, the diffusion coefficient of electron is significantly slowed down, due to the exponential growth of the trapping/detrapping events.

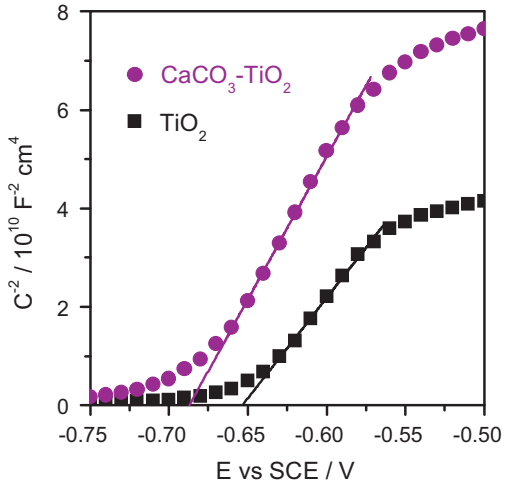

Fig. 7. Mott-Schottky curves for the blank and $CaCO_3$ coated electrodes.

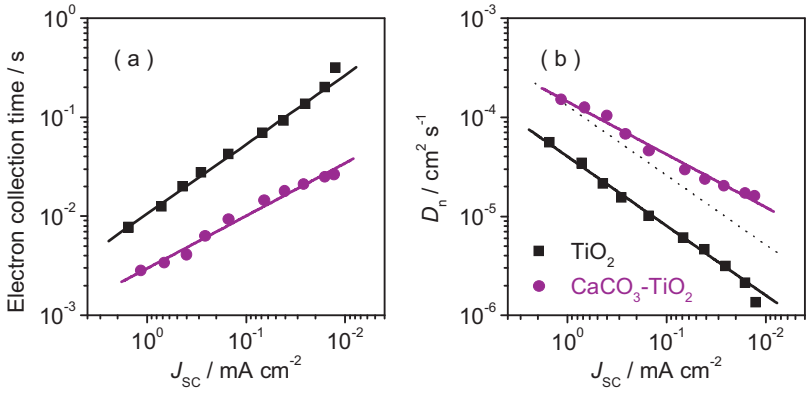

Fig. 8. Effect of cured calcareous coatings on electronic properties of the semiconductor electrodes. Electron collection time constants (a) and electron-diffusion coefficient (b) derived from the transient measurements at the short-circuit conditions. In order to mainly distinguish the contribution from the promotion of interparticle connectivity and from the reduction of electronic traps, the plot of the blank electrode was parallel translated to the high current side of the plot of the cured electrode (black thin dot line) (b).

For the blank electrode, the decrease in the diffusion coefficient over the J_{SC} range is much rapider, as compared with that of the cured electrode. The difference in the value of D_n of the two electrodes becomes larger, as the photocurrent density falling. The continuous increase in the difference of charge diffusion parameters over the variation (decrease) of J_{SC} for the two electrodes reveal that the influence of trap states on the charge transport is rather different for the two electrodes. The relatively low slope in the D_n–J_{SC} plots (Fig. 8(b)) suggests that the probability of trapping/detrapping events during the charge transport procedure is relatively low and the trapping-mediated electronic process is less dominant in the cured electrode.

4.3.2. Lifetime of electrons in semiconductor electrodes

As it has been proven, the charge transport procedures are strongly depending on the density and distribution of electronic states localized in the bandgap of the semiconductor [41–50]. We have also revealed that the probability of trapping/detrapping events can be reduced by introduction of calcareous coatings into the electrode. It is therefore of great importance to investigate the trapping-mediated electronic process of interfacial charge recombination dynamics in the two electrodes.

The electron lifetime, τ_n in DSSC is a central quantity to determine the interfacial charge recombination dynamics in the cell, and it is a strong function of the Fermi level or the open-circuit voltage (V_{OC}). The time constant is influenced not only by the rate constant for direct charge transfer from the conduction band to the solution, but also by the distribution of electronic states and electronic transitions that intervene in operation of the cells [51]. According to the quasi-static treatment developed by Bisquert and Vikhrenko [49], in a certain potential range, the apparent electron lifetime is related to the conduction band electron lifetime by the expression [49,51]:

$$\tau_n = \left(\frac{\partial n_t}{\partial n_c}\right)\tau_0 \quad (5)$$

in which n_t is the trapped electron density, n_c is the conduction band electron density, τ_0 is the inverse of the pseudo-first-order rate for back transfer of electrons from the conduction band. By comparing the two equations (Eqs. (4) and (5)), it can be seen that the factors in τ_n and D_n obey a reciprocal relation. Clearly, the electron lifetime in this potential range is also a consequence of trapping and detrapping of electrons at sites located in the bandgap of the semiconductor.

The relationship between the electron lifetime and V_{OC} suggests that the introduction of calcareous coatings on the surface of the semiconductor film play a crucial role to the interfacial charge transfer (Fig. 9). In the more negative potential side, the charge recombination dynamics is controlled by the transfer of the conduction band electrons [51]. The values of τ_n for the cured electrode is nearly one order of magnitude larger than that the case of the blank one, suggests that the formed calcareous barrier layers on the surface of the TiO$_2$ nanoparticles can effectively prevent the charge transfer (recombination) between the conduction band electrons and the oxidized species in the electrolyte, which is in good agreement with the impedance observation (Fig. 6).

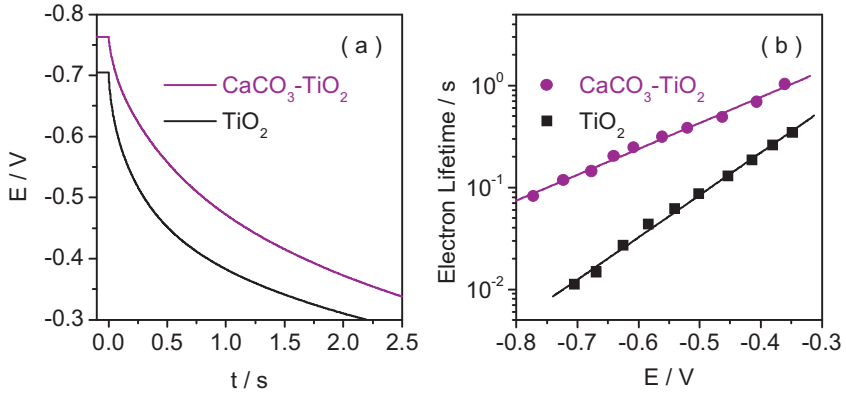

Fig. 9. Effect of cured calcareous coatings on electronic properties of the semiconductor electrodes. Open-circuit voltage decay patterns (a) and related electron lifetime constants (b) for the cells with blank and cured electrodes.

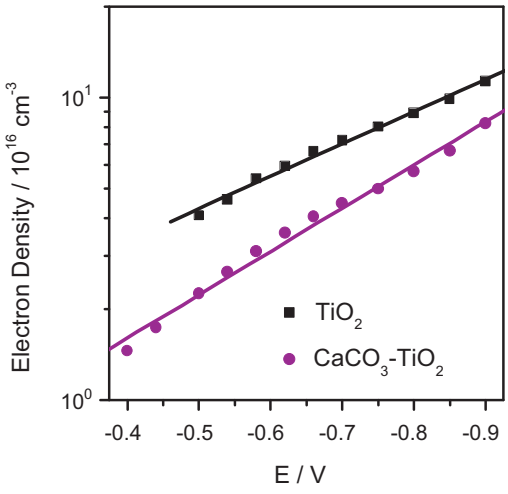

Fig. 10. Densities of trapped electrons in the TiO_2 electrodes with and without calcareous coatings.

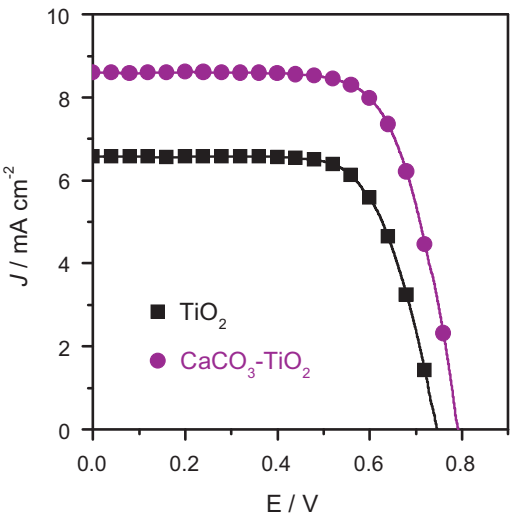

Fig. 11. Effect of $CaCO_3$ coatings on the photovoltaic characteristics of DSSCs.

As the electrode potentials become less negative, the charge recombination between the electrons and the oxidized species is gradually dominated by the internal trapping and detrapping [51]. In this range, the variation (increase) of the values of τ_n with potential for the blank electrode is obvious, as compared with that of the cured one (Fig. 9(b)).

The significant growth in the time constant for interfacial charge recombination in the blank electrode should be ascribed to two factors. The first reason is that with the Fermi level shifting toward lower energy position, the increase in the density of unoccupied trap states in the bandgap of the blank electrode is much more significant, as compared with that of the cured one, provides more trap sites and increases the probability of traping/detrapping events for the electron [51]. The second is that the time constant for the thermal release of trapped electrons to the conduction band become larger, as the trap states are localized in deep levels.

4.3.3. Strain-induced reduction of trap states

As described above, trapping/detrapping events play a crucial role in both electronic processes of the charge transport in the semiconductor electrodes and interfacial charge transfer on SEI. The exponential growth of the electron lifetime over the electrode potential as well as the exponential variation of the electron collection time constants and the electron diffusion coefficient over the intensity of the photocurrent reveals that the trap states in the band gap of the semiconductor are exponentially distributed. For the cured electrode, the relatively lower slope of the plots in both the relationships of τ_n–V and D_n–J_{SC} suggests that the effect of trapping/detrapping events on the electronic processes is less dominant, as compared with that of the blank one (Figs. 8 and 9). According to the MT framework [43,44], the low probability of the trapping/detrapping events means the density of the electronic states in the bandgap of the semiconductor is relatively low.

In order to confirm the change in the density of the electronic states in the bandgap of the semiconductor, transient technique was employed to determine the number of trapped charges (electrons) in the electrodes. Fig. 10 presents the density of trapped electrons at various bias potentials of the cells. As it shown, the density of the trapped electrons increased exponentially as the potential shifts toward more negative values. For the cured electrode, the density of electrons is much lower than that of that of the blank one, indicates that the density of trap states in the bandgap of the semiconductor becomes lower after the calcareous coatings were applied onto the surface of the electrode.

To the best of our knowledge, promotion of charge transport in semiconductor by surface coating has not been reported yet, and the detail mechanism for this phenomenon is still unclear. The facile charge transport in the cured electrode should be attributed to the decrease in the density of trap sites in the bandgap and the improvement in the interparticle contact condition of the semiconductor, resulting most likely from the compression stress generated from the phase conversion of the calcareous coating.

4.4. Photovoltaic performance

By virtue of the compression stress resulting from the cured calcareous coatings on the surface of the electrodes, the interparticle electronic connectivity is improved and the density of trap states in the nanoparticles is reduced. All of these can facilitate the electron transport in semiconductor electrodes. Moreover, the formed $CaCO_3$ coatings can protect the electrons from recombination. Therefore, it is expected that the result DSSCs with these electrodes would possess better photovoltaic performance. Fig. 11 shows the photocurrent–voltage characteristics of the cells. It is clear that the photovoltaic behaviors of the cell significantly changed when the semiconductor electrode was modified by the cured $CaCO_3$ coatings. Under one sun illumination, the photovoltaic parameters including open-circuit voltage (V_{OC}), short-circuit photocurrent density (J_{SC}), fill factor (*FF*), and overall energy conversion efficiency (η) for the cell with blank TiO_2 electrode are 749 mV, 6.57 mA/cm^2, 0.696, and 3.43%, respectively. The corresponding values (V_{OC}, J_{SC}, and *FF*) for the cured cell are respectively 788 mV, 8.59 mA/cm^2, and 0.708, and the value of η becomes 4.79%, which is ~40% larger than that of the blank one.

5. Conclusion

In summary, we have developed a new strategy for low-temperature fabrication of dye-sensitized solar cells by SILAR of $Ca(OH)_2$ and curing the calcareous coating into $CaCO_3$ in the presence of CO_2. The strain resulting from the phase transformation of the calcareous coating can promote the electronic connectivity between individual particles and reduce the density of the trap states in the bandgap of the semiconductors, which can facilitate the transport of electrons in the semiconductor electrodes and increase the electron diffusion coefficient. Besides, the $CaCO_3$ coatings on the surface of the TiO_2 electrodes can shift the conduction band edge toward higher energy level and prevent the

photogenerated electrons from recombination. By virtue of these excellent characteristics, an increment of 40% in energy conversion efficiency is achieved.

Acknowledgements

J. Chen thanks Dr. Yinghua Xu (Zhejiang Univ. Technol.) and Dr. Tiancheng Xu (HzCell Electrochem. Corp.) for the help on the discussion of the charge transport project.

References

[1] B. Oregan, M. Gratzel, A low-cost, high-efficiency solar-cell based on dye-sensitized colloidal TiO_2 films, Nature 353 (1991) 737.
[2] M. Gratzel, Photoelectrochemical cells, Nature 414 (2001) 338.
[3] A. Yella, H.-W. Lee, H.N. Tsao, C. Yi, A.K. Chandiran, M.K. Nazeeruddin, E.W.-G. Diau, C.-Y. Yeh, S.M. Zakeeruddin, M. Grätzel, Porphyrin-sensitized solar cells with cobalt (II/III)-based redox electrolyte exceed 12 percent efficiency, Science 334 (2011) 629.
[4] B.E. Hardin, H.J. Snaith, M.D. McGehee, The renaissance of dye-sensitized solar cells, Nature Photonics 6 (2012) 162.
[5] F. Pichot, J.R. Pitts, B.A. Gregg, Low-temperature sintering of TiO_2 colloids: application to flexible dye-sensitized solar cells, Langmuir 16 (2000) 5626.
[6] N.G. Park, K.M. Kim, M.G. Kang, K.S. Ryu, S.H. Chang, Y.J. Shin, Chemical sintering of nanoparticles: a methodology for low-temperature fabrication of dye-sensitized TiO_2 films, Advanced Materials 17 (2005) 2349.
[7] X. Zhao, H. Lin, X. Li, J. Li, The influence of nitric acid on electron transport and recombination for non-sintering TiO_2 photoanodes, Electrochimica Acta 67 (2012) 62.
[8] P. Zhang, C. Wu, Y. Han, T. Jin, B. Chi, J. Pu, L. Jian, Low-temperature preparation of hierarchical structure TiO_2 for flexible dye-sensitized solar cell, Journal of the American Ceramic Society 95 (2012) 1372.
[9] P.M. Sirimanne, H.C. Weerasinghe, G.P. Simon, Y.B. Cheng, Preparation of chemically sintered ZnO films and their application in dye sensitized solar cells formed on plastic substrates, Journal of Photochemistry and Photobiology A: Chemistry 228 (2012) 15.
[10] H. Lee, D. Hwang, S.M. Jo, D. Kim, Y. Seo, D.Y. Kim, Low-temperature fabrication of TiO_2 electrodes for flexible dye-sensitized solar cells using an electrospray process, ACS Applied Materials & Interfaces 4 (2012) 3308.
[11] F. Hu, Y. Xia, Z. Guan, X. Yin, T. He, Low temperature fabrication of ZnO compact layer for high performance plastic dye-sensitized ZnO solar cells, Electrochimica Acta 69 (2012) 97.
[12] X. Yin, Z. Xue, L. Wang, Y. Cheng, B. Liu, High-performance plastic dye-sensitized solar cells based on low-cost commercial P25 TiO_2 and organic dye, ACS Applied Materials & Interfaces 4 (2012) 1709.
[13] D.S. Zhang, T. Yoshida, H. Minoura, Low-temperature fabrication of efficient porous titania photoelectrodes by hydrothermal crystallization at the solid/gas interface, Advanced Materials 15 (2003) 814.
[14] Y. Li, W. Lee, D.-K. Lee, K. Kim, N.-G. Park, M.J. Ko, Pure anatase TiO_2 nanoglue: an inorganic binding agent to improve nanoparticle interconnections in the low-temperature sintering of dye-sensitized solar cells, Applied Physics Letters 98 (2011) 103301.
[15] H.C. Weerasinghe, P.M. Sirimanne, G.P. Simon, Y.B. Cheng, Cold isostatic pressing technique for producing highly efficient flexible dye-sensitised solar cells on plastic substrates, Progress in Photovoltaics 20 (2012) 321.
[16] T. Yamaguchi, N. Tobe, D. Matsumoto, H. Arakawa, Highly efficient plastic substrate dye-sensitized solar cells using a compression method for preparation of TiO_2 photoelectrodes, Chemical Communications (2007) 4767.
[17] S.A. Haque, E. Palomares, H.M. Upadhyaya, L. Otley, R.J. Potter, A.B. Holmes, J.R. Durrant, Flexible dye sensitised nanocrystalline semiconductor solar cells, Chemical Communications (2003) 3008.
[18] L. Grinis, S. Kotlyar, S. Ruhle, J. Grinblat, A. Zaban, Conformal nano-sized inorganic coatings on mesoporous TiO_2 films for low-temperature dye-sensitized solar cell fabrication, Advanced Functional Materials 20 (2010) 282.
[19] T.A.N. Peiris, S. Senthilarasu, K.G.U. Wijayantha, Enhanced performance of flexible dye-sensitized solar cells: electrodeposition of $Mg(OH)_2$ on a nanocrystalline TiO_2 electrode, Journal of Physical Chemistry C 116 (2011) 1211.
[20] V.S. Ramachandran, R.F. Feldman, Length change characteristics of $Ca(OH)_2$ compacts on exposure to water vapour, Journal of Applied Chemistry 17 (1967) 328.
[21] P.J. Sereda, V.S. Ramachandran, Predictability gap between science and technology of cements: II. Physical and mechanical behavior of hydrated cements, Journal of the American Ceramic Society 58 (1975) 249.
[22] E.G. Swenson, P.J. Sereda, Mechanism of the carbonatation shrinkage of lime and hydrated cement, Journal of Applied Chemistry 18 (1968) 111.
[23] Y.F. Houst, Proc. 4th CANMET/ACI International Conference on Durability of Concrete, Ottawa, Canada, 1997.
[24] Z.S. Wang, M. Yanagida, K. Sayama, H. Sugihara, Electronic-insulating coating of $CaCO_3$ on TiO_2 electrode in dye-sensitized solar cells: Improvement of electron lifetime and efficiency, Chemistry of Materials 18 (2006) 2912.
[25] S. Lee, J.Y. Kim, S.H. Youn, M. Park, K.S. Hong, H.S. Jung, J.K. Lee, H. Shin, Preparation of a nanoporous $CaCO_3$-coated TiO_2 electrode and its application to a dye-sensitized solar cell, Langmuir 23 (2007) 11907.
[26] H.C. Weerasinghe, P.M. Sirimanne, G.P. Simon, Y.B. Cheng, Fabrication of efficient solar cells on plastic substrates using binder-free ball milled titania slurries, Journal of Photochemistry and Photobiology A: Chemistry 206 (2009) 64.
[27] A. Zaban, M. Greenshtein, J. Bisquert, Determination of the electron lifetime in nanocrystalline dye solar cells by open-circuit voltage decay measurements, ChemPhysChem 4 (2003) 859.
[28] S. Nakade, T. Kanzaki, Y. Wada, S. Yanagida, Stepped light-induced transient measurements of photocurrent and voltage in dye-sensitized solar cells: application for highly viscous electrolyte systems, Langmuir 21 (2005) 10803.
[29] N.W. Duffy, L.M. Peter, R.M.G. Rajapakse, K.G.U. Wijayantha, A novel charge extraction method for the study of electron transport and interfacial transfer in dye sensitised nanocrystalline solar cells, Electrochemistry Communications 2 (2000) 658.
[30] K. Sunahara, J. Ogawa, S. Mori, A method to measure electron lifetime in dye-sensitized solar cells: stepped current induced measurement of cell voltage in the dark, Electrochemistry Communications 13 (2011) 1420.
[31] B. Li, J.Z. Chen, J.F. Zheng, J.H. Zhao, Z.P. Zhu, H.W. Jing, Photovoltaic performance enhancement of dye-sensitized solar cells by formation of blocking layers via molecular electrostatic effect, Electrochimica Acta 59 (2012) 207.
[32] Q. Wang, Z. Zhang, S.M. Zakeeruddin, M. Gratzel, Enhancement of the performance of dye-sensitized solar cell by formation of shallow transport levels under visible light illumination, Journal of Physical Chemistry C 112 (2008) 7084.
[33] J. Bisquert, Theory of the impedance of electron diffusion and recombination in a thin layer, Journal of Physical Chemistry B 106 (2001) 325.
[34] F. Fabregat-Santiago, G. Garcia-Belmonte, J. Bisquert, A. Zaban, P. Salvador, Decoupling of transport, charge storage, and interfacial charge transfer in the nanocrystalline TiO_2/electrolyte system by impedance methods, Journal of Physical Chemistry B 106 (2002) 334.
[35] F. Fabregat-Santiago, J. Bisquert, G. Garcia-Belmonte, G. Boschloo, A. Hagfeldt, Influence of electrolyte in transport and recombination in dye-sensitized solar cells studied by impedance spectroscopy, Solar Energy Materials and Solar Cells 87 (2005) 117.
[36] F. Fabregat-Santiago, J. Bisquert, E. Palomares, L. Otero, D.B. Kuang, S.M. Zakeeruddin, M. Gratzel, Correlation between photovoltaic performance and impedance spectroscopy of dye-sensitized solar cells based on ionic liquids, Journal of Physical Chemistry C 111 (2007) 6550.
[37] J. Bandara, U.W. Pradeep, Tuning of the flat-band potentials of nanocrystalline TiO_2 and SnO_2 particles with an outer-shell MgO layer, Thin Solid Films 517 (2008) 952.
[38] M.H. Kim, Y.U. Kwon, Semiconductor, CdO as a blocking layer material on DSSC electrode: mechanism and application, Journal of Physical Chemistry C 113 (2009) 17176.
[39] P. Moulin, H. Roques, Zeta potential measurement of calcium carbonate, Journal of Colloid and Interface Science 261 (2003) 115.
[40] R. Memming, Semiconductor Electrochemistry, Wiley-VCH, Weinheim, 2001.
[41] J. Bisquert, Physical electrochemistry of nanostructured devices, Physical Chemistry Chemical Physics 10 (2008) 49.
[42] K. Schwarzburg, F. Willig, Influence of trap filling on photocurrent transients in polycrystalline TiO_2, Applied Physics Letters 58 (1991) 2520.
[43] T. Tiedje, J.M. Cebulka, D.L. Morel, B. Abeles, Evidence for exponential band tails in amorphous silicon hydride, Physical Review Letters 46 (1981) 1425.
[44] J. Orenstein, M. Kastner, Photocurrent transient spectroscopy: measurement of the density of localized states in α-As_2Se_3, Physical Review Letters 46 (1981) 1421.
[45] A.C. Fisher, L.M. Peter, E.A. Ponomarev, A.B. Walker, K.G.U. Wijayantha, Intensity dependence of the back reaction and transport of electrons in dye-sensitized nanacrystalline TiO_2 solar cells, Journal of Physical Chemistry B 104 (2000) 949.
[46] J.P. Gonzalez-Vazquez, J.A. Anta, J. Bisquert, Determination of the electron diffusion length in dye-sensitized solar cells by random walk simulation: Compensation effects and voltage dependence, Journal of Physical Chemistry C 114 (2010) 8552.
[47] W.H. Leng, P.R.F. Barnes, M. Juozapavicius, B.C. O'Regan, J.R. Durrant, Electron diffusion length in mesoporous nanocrystalline TiO_2 photoelectrodes during water oxidation, Journal of Physical Chemistry Letters 1 (2010) 967.
[48] J. van de Lagemaat, A.J. Frank, Effect of the surface-state distribution on electron transport in dye-sensitized TiO_2 solar cells: nonlinear electron-transport kinetics, Journal of Physical Chemistry B 104 (2000) 4292.
[49] J. Bisquert, V.S. Vikhrenko, Interpretation of the time constants measured by kinetic techniques in nanostructured semiconductor electrodes and dye-sensitized solar cells, Journal of Physical Chemistry B 108 (2004) 2313.
[50] J. Bisquert, Chemical diffusion coefficient of electrons in nanostructured semiconductor electrodes and dye-sensitized solar cells, Journal of Physical Chemistry B 108 (2004) 2323.
[51] J. Bisquert, A. Zaban, M. Greenshtein, I. Mora-Sero, Determination of rate constants for charge transfer and the distribution of semiconductor and electrolyte electronic energy levels in dye-sensitized solar cells by open-circuit photovoltage decay method, Journal of the American Chemical Society 126 (2004) 13550.